*Elements of Photonics, Volume II: For Fiber and Integrated Optics*. Keigo Iizuka

ISBNs: 0-471-40815-8 (Hardback); 0-471-22137-6 (Electronic)

# 10

# OPTICAL WAVEGUIDES AND DEVICES FOR INTEGRATED OPTICS

In integrated optics, an optical element can be fabricated on a substrate the size of a microscope deck glass. Such elements as lenses, light deflectors, or the optical spectrum analyzer need to confine the light beam only in one dimension and the slab optical guide is widely used. However, other elements, such as the directional coupler, optical modulators, a laser diode cavity, and mode filters, need an optical guide that can confine the light in two dimensions. In this chapter, a rectangular optical guide that confines the light both in the $x$ and $y$ directions and transmits in the $z$ direction is described.

The formulas developed in the previous chapter will be used freely and we highly recommend that you thoroughly review Chapter 9 before proceeding to this chapter. The latter part of this chapter also incorporates concepts from Chapter 5 on electrooptic media.

## 10.1 RECTANGULAR OPTICAL WAVEGUIDE

A rectangular guide [1–4] with the geometry shown in Fig. 10.1 is considered. The thickness is $2d$, and the width is $2w$. The indices of refraction $n_2$, $n_3$, $n_4$, $n_5$ of the cladding medium are not necessarily the same but are all smaller than $n_1$ of the core region.

### 10.1.1 Assumptions

The only means to confine the component waves inside the optical waveguide is total internal reflection at the boundaries. Unlike microwave waveguides, optical waveguides do not have metal walls to confine the lightwave. There are many similarities in the behavior of the modes between microwave and optical guides, but there are also differences.

In order to make the analysis manageable, certain assumptions have to be made. The first assumption is that the difference in the indices of refraction of the cladding

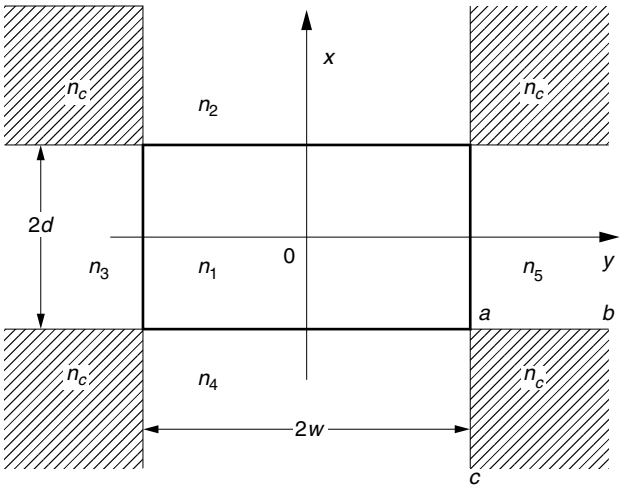


**Figure 10.1** Geometry of the rectangular optical guide.

and the core is small so that all the guided component waves make a small angle with the $z$ axis.

This assumption needs some further explanation. In Section 9.2, the assumption that $H_z = 0$ was necessary to simplify the wave equation. All the solutions so far are based on this assumption. However, the assumption that $H_z = 0$ cannot hold true in the rectangular optical waveguide. In the planar cases mentioned in the previous chapter, the component waves took a zigzag path only in the $x$ direction, as shown in Fig. 10.2a, and $H_z = 0$ was possible. When the component waves take a zigzag path in both the $x$ and $y$ directions to satisfy the boundary conditions on both walls as indicated in Fig. 10.2b, the **H** component cannot be parallel to the $y$ direction and at the same time remain perpendicular to the direction of propagation. The **H** component has to be like $H_y'$ shown by the dotted line in Fig. 10.2b. But as long as the angle of the zigzag is small, the approximation

$$H_y \doteqdot H_y' \tag{10.1}$$

can be made.

We will still use the results in Section 9.2 as approximate expressions, and we will call the modes associated with $H_y'$ the "TM-like modes." The common convention for designating the modes in a rectangular guide is different from what we have been using for the slab guide. In rectangular guides, the designation is with reference to the transverse **E** field. Recall that the TM mode of the slab guide had only three nonzero components: $H_y$, $E_x$, and $E_z$ as in Eq. (9.23). The "TM-like modes" of the rectangular guide are called the $E^x$ modes and their mode numbers are designated by the number of the extrema rather than an integer $\mu$ associated with the dispersion equation as in Eq. (9.146). The mode with $p$ extrema in the $x$ direction and $q$ extrema in the $y$ direction is designated by $E_{pq}^x$.

The TE mode of the slab guide again has only three nonzero components: $E_y$, $H_x$, and $H_z$ as in Eq. (9.56). The "TE-like modes" of the rectangular guide are designated by $E_{pq}^y$.

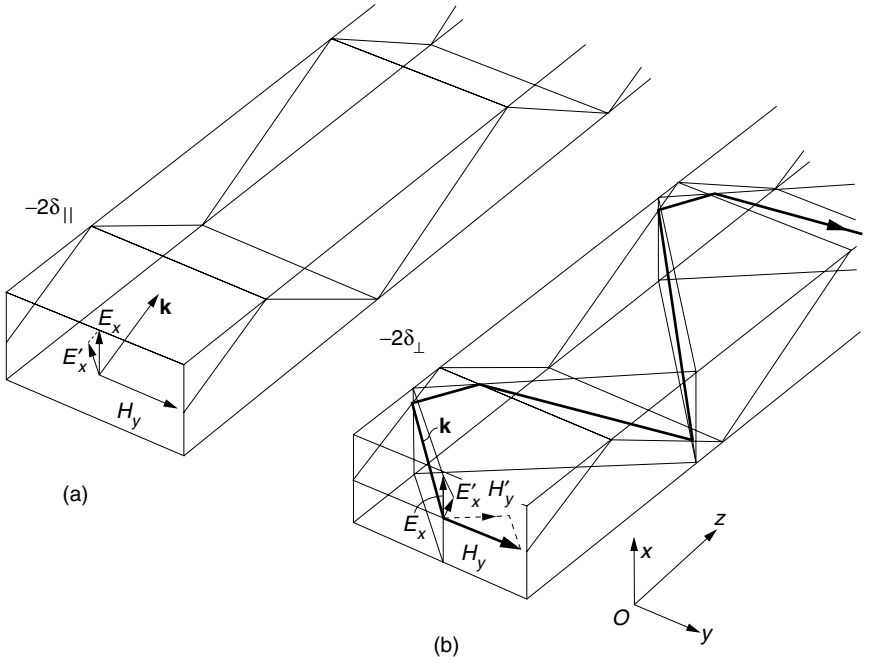


**Figure 10.2** Ray path of ''TM-like mode'' or ''$E^x_{pq}$ mode.'' (a) Zigzag only in the $x$ direction. (b) Zigzag in both $x$ and $y$ directions.

Throughout the calculations, the boundary conditions associated with the hatched areas in Fig. 10.1 have been ignored. If one attempts to find a solution including, for example, the lower right hatched region, first a general solution has to be found that matches the boundaries along both a–c and a–b, and then the continuity boundary conditions have to be applied so that the solution in the hatched region connects with the decay function $\gamma_4$ along a–c and with the decay function $\gamma_5$ along a–b. Now, $\gamma_4$ is connected with $K_x$ by a characteristic equation, and $\gamma_5$ is connected with $K_y$ by another characteristic equation. Inclusion of the hatched region means that $K_x$ and $K_y$ are no longer independent, as has been assumed up to now. Furthermore, $K_x$ and $K_y$ are coupled in a very complicated manner (coupled equations). By ignoring the hatched regions, we are making the assumption that $K_x$ and $K_y$ can be chosen independently. Since the hatched areas are bordered by regions containing evanescent waves, which are much smaller in amplitude than the propagated wave, the hatched regions may be ignored without serious error.

An additional assumption made on the hatched region in Fig. 10.1 is explained in the boxed note.

### 10.1.2 Characteristic Equation for the Rectangular Guide

Now, the characteristic equation for the "TM-like mode" or $E^x_{pq}$ mode will be derived. The method of the modified ray model will be used. Unlike a slab guide, the dimensions of the rectangular core are finite in both the $x$ and $y$ directions and standing waves (modes) exist in both the $x$ and $y$ directions. Let the propagation constants in the $x$

and $y$ directions be $K_x$ and $K_y$, respectively. The analysis is quite similar to the slab guide except that the dispersion equation has to be satisfied in both $x$ and $y$ directions.

The dispersion equation for the zigzag path shown in Fig. 10.2a is considered first. The field component $E_x$ is in the plane of propagation and Eq. (2.91) is used for the phase shift due to reflection, similar to the derivation of Eq. (9.146) for the planar guide.

$$4K_x d - 2\tan^{-1}\left(\frac{\gamma_2}{n_2'^2 K_x}\right) - 2\tan^{-1}\left(\frac{\gamma_4}{n_4'^2 K_x}\right) = 2\mu\pi \tag{10.2}$$

where

$$n_2' = \frac{n_2}{n_1}, \qquad n_4' = \frac{n_4}{n_1} \tag{10.3a}$$

$$\mu = p - 1 \tag{10.3b}$$

$$K_x = \sqrt{(n_1 k)^2 - \beta^2 - K_y^2} \tag{10.3c}$$

$K_y$ accounts for the inclusion of the $\partial^2 H_y/\partial y^2$ term in Eq. (9.5). Note the relationship between $\mu$ and $p$. Equation (10.2) can be reduced to the dominant mode, the $TM_0$ mode, with $n_2' = n_4'$ and $\mu = 0$. The $TM_0$ mode has one intensity maximum in the $x$ direction. Thus, if $p$ represents the number of intensity maxima, then $\mu$ must be replaced by $p - 1$.

The attenuation constants of the evanescent waves in the upper and lower cladding layers are

$$\gamma_2 = \sqrt{\beta^2 + K_y^2 - (n_2 k)^2} \tag{10.4}$$

$$\gamma_4 = \sqrt{\beta^2 + K_y^2 - (n_4 k)^2} \tag{10.5}$$

Now consider the $y$ direction and the left–right zigzag path shown in Fig. 10.2b. In this case, $E_x$ is perpendicular to the plane of the light path and Eq. (2.92) is used instead of Eq. (2.91). The dispersion equation for the left–right zigzag path is

$$4K_y w - 2\tan^{-1}\left(\frac{\gamma_3}{K_y}\right) - 2\tan^{-1}\left(\frac{\gamma_5}{K_y}\right) = 2\nu\pi \tag{10.6}$$

where $\nu = q - 1$

$$K_y = \sqrt{(n_1 k)^2 - \beta^2 - K_x^2} \tag{10.7}$$

and

$$\gamma_3 = \sqrt{\beta^2 + K_x^2 - (n_3 k)^2} \tag{10.8}$$

$$\gamma_5 = \sqrt{\beta^2 + K_x^2 - (n_5 k)^2} \tag{10.9}$$

So far, seven unknowns — $K_x$, $K_y$, $\gamma_2$, $\gamma_3$, $\gamma_4$, $\gamma_5$, and $\beta$ — have been generated.

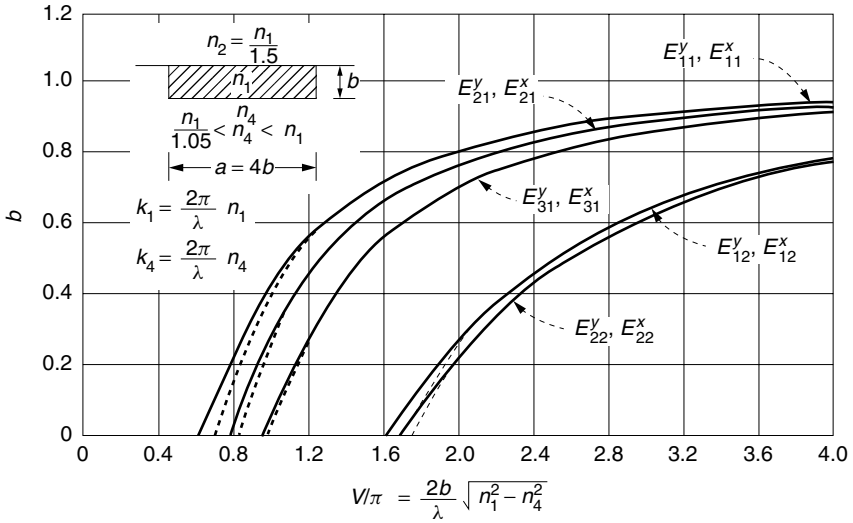


**Figure 10.3** Propagation constants for different modes with respect to the dimension of the optical guide. Dispersion curves are shown for an embedded guide with height $b$ and width $a = 4b$. The refractive index of the embedded guide is $n_1$, the refractive index of the medium above the guide is $n_2 = n_1/1.5$, and the refractive index of the embedding medium is $n_4$. The vertical axis is the normalized guide index $b$ defined as $b = (N^2 - n_4^2)/(n_1^2 - n_4^2)$. $N$ is the effective index of refraction. The horizontal axis is the normalized thickness $V$ divided by $\pi$: $V/\pi = (2b/\lambda)\sqrt{n_1^2 - n_4^2}$. (After E. A. J. Marcatili [5] with $x$ and $y$ conventions interchanged to match the notation in this textbook.)

There are eight equations, Eqs. (10.2) through (10.9), but note that Eqs. (10.3c) and (10.7) are identical so that there are exactly the seven needed independent equations. They are transcendental equations and the solutions are obtainable only by numerical methods. The results obtained by Marcatili [5] are shown in Fig. 10.3.

For a given $V$, the value of $b$ is found from the graph. From the normalized guide index $b$, the effective index of refraction $N$ is calculated using

$$b = \frac{N^2 - n_4^2}{n_1^2 - n_4^2} \tag{10.10}$$

The propagation constant $\beta$ of such a guide is found from $N$ as

$$\beta = kN \tag{10.11}$$

Now, in order to clarify all the above descriptions a practical example is in order.

### 10.1.3 A Practical Example

Many practical devices can be generated from the geometry shown in Fig. 10.4. The next example explores some characteristics of a guide of this geometry for typical physical constants.

**Example 10.1** An optical guide such as the one shown in Fig. 10.4 is called an embedded or buried guide. For the "TM-like modes," or $E_{pq}^x$ modes, find (a) the

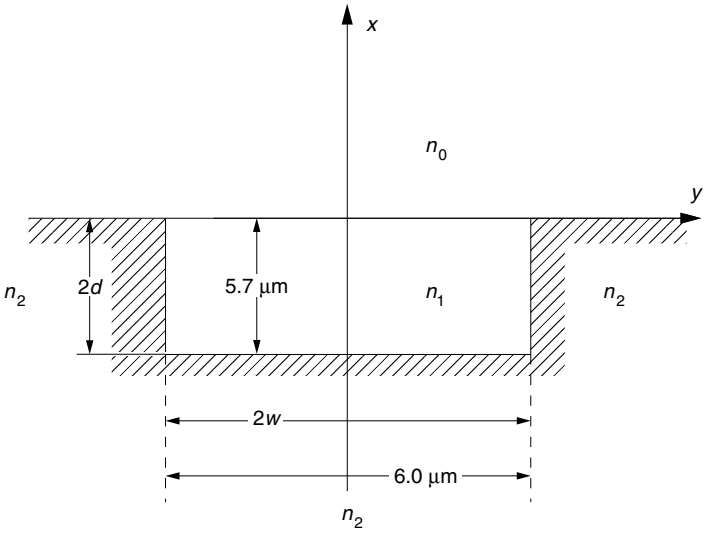


**Figure 10.4** Geometry of a buried optical guide.

characteristic equation, (b) the propagation constant and the cutoff of the lowest order mode, and (c) the field distribution of each mode. The physical constants are

$$n_1 = 1.55, \quad n_2 = 1.54, \quad 2d = 5.7\ \mu\text{m}, \quad 2w = 6.0\ \mu\text{m}, \quad \lambda = 1.3\ \mu\text{m}$$

***Solution*** Figure 10.4 is an asymmetric guide in the $x$ direction, whereas it is a symmetric guide in the $y$ direction. The solution can be obtained by combining the earlier results for each geometry.

The dispersion equations in the $y$ direction are, from Eq. (10.6),

$$\tan K_y w = \frac{\gamma_2}{K_y} \quad \text{for even } \nu \tag{10.12}$$

$$-\cot K_y w = \frac{\gamma_2}{K_y} \quad \text{for odd } \nu \tag{10.13}$$

where

$$K_y = \sqrt{(n_1 k)^2 - \beta^2 - K_x^2} \tag{10.14}$$

$$\gamma_2 = \sqrt{\beta^2 + K_x^2 - (n_2 k)^2} \tag{10.15}$$

From Eqs. (10.14) and (10.15), we have

$$(K_y w)^2 + (\gamma_2 w)^2 = V_w^2 \tag{10.16}$$

$$V_w = kw\sqrt{n_1^2 - n_2^2} \tag{10.17}$$

From Fig. 9.2 with $V_w = 0.811\pi$, the $TM_0$ and $TM_1$ modes can be excited in the $y$ direction. The corresponding $K_y w$ values are

$$\begin{aligned} K_{y0}w &= 0.37\pi \\ K_{y1}w &= 0.70\pi \end{aligned} \tag{10.18}$$

An approximate dispersion equation in the $x$ direction is, from Eq. (9.157),

$$-\cot 2K_x d = \frac{\gamma_2}{n_2'^2 K_x} \tag{10.19}$$

and

$$(\gamma_2 d)^2 + (K_x d)^2 = V_d^2 \tag{10.20}$$

$$V_d = kd\sqrt{n_1^2 - n_2^2} \tag{10.21}$$

Figure 9.16 is used with $V_d = 0.77\pi$. In the $x$ direction again there are two modes:

$$\begin{aligned} K_{x0}d &= 0.42\pi \quad \text{for } TM_0 \\ K_{x1}d &= 0.76\pi \quad \text{for } TM_1 \end{aligned} \tag{10.22}$$

Now, the modes for the two directions are combined. First, the modes will be expressed using the notation of $E_{pq}^x$, where $p$ and $q$ represent the number of the extrema for the $x$ and $y$ directions. The $TM_0$ mode has one and the $TM_1$ has two extrema. In terms of $E_{pq}^x$, the available modes are $E_{11}^x$, $E_{12}^x$, $E_{21}^x$, and $E_{22}^x$. The propagation constant of the lowest order mode $E_{11}^x$ is, from Eq. (10.14),

$$\beta_{11} = \sqrt{(n_1 k)^2 - (K_{x0})^2 - (K_{y0})^2} \tag{10.23}$$

With the results in Eqs. (10.18) and (10.22) combined with the values of $w$ and $d$, the propagation constant of $E_{11}^x$ is

$$\beta_{11} = 7.46 \text{ rad}/\mu\text{m} \tag{10.24}$$

The cutoff condition for the $E_{11}^x$ mode is determined by the asymmetric mode alone because the cutoff of the symmetric mode is $V = 0$. The cutoff for the asymmetric mode is $V_d = \pi/4$.

$$2d_c = \frac{\lambda}{4\sqrt{n_1^2 - n_2^2}} = 1.85 \ \mu\text{m} \tag{10.25}$$

Combining the distributions in the $x$ and $y$ directions, the field distribution shown in Fig. 10.5 is obtained in a manner similar to that described in Section 9.4. □

## 10.2 EFFECTIVE INDEX METHOD FOR RECTANGULAR OPTICAL GUIDES

The effective index method [6,7] is simple and useful for finding an approximate expression for the propagation constant of a rectangular optical guide. The effective index method is conceptually more straightforward than what was explained in the previous section and provides almost identical results. The method is explained

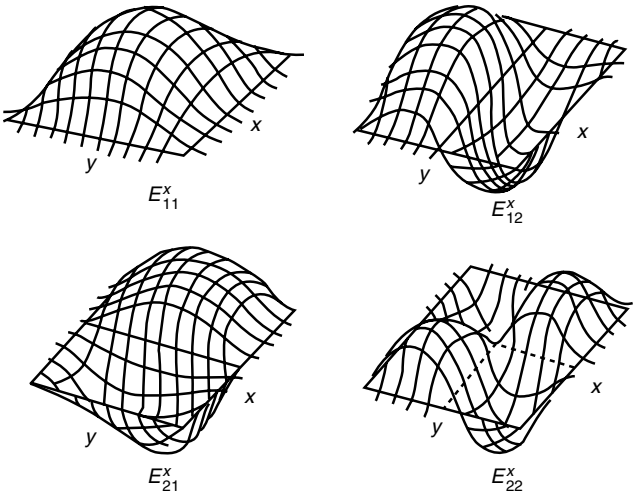


**Figure 10.5** Mode patterns in a rectangular guide.

using the rectangular optical guide shown in Fig. 10.6a, which was dealt with in Example 10.1. The procedure consists of two steps; each step involves finding the propagation constant of a slab optical guide of an infinite extent. The first step is to find the propagation constant $\beta_w$ of a slab optical guide with thickness $2w$ as shown in Fig. 10.6b. The second step is to calculate the propagation constant $\beta_{wd}$ of the slab optical guide with thickness $2d$, but using the effective index of refraction $N = \beta_w/k$ obtained in the first step as the index of refraction of the core layer, as shown in Fig. 10.6c. The propagation constant $\beta_{wd}$ of the second optical guide is the desired propagation constant of the rectangular optical guide.

**Step 1.** With the geometry of the first slab optical guide shown in Fig. 10.6b, the propagation constant is found. Assuming even TM modes, the characteristic equation, from Eqs. (9.26) and (9.27), is

$$n^2 Kw \tan Kw = \gamma w \tag{10.26}$$

with

$$(Kw)^2 + (\gamma w)^2 = V_w^2 \tag{10.27}$$

where

$$V_w = kw\sqrt{n_1^2 - n_2^2}$$

The intersections of the two curves provide the solutions. Let's say one of the solutions is $K_y$. Then, the propagation constant $\beta_w$ is, from Eq. (9.6),

$$\beta_w^2 = (n_1 k)^2 - K_y^2 \tag{10.28}$$

and the effective index of refraction $N$ is, from Eq. (9.44),

$$N_1^2 = \frac{(n_1 k)^2 - K_y^2}{k^2} \tag{10.29}$$

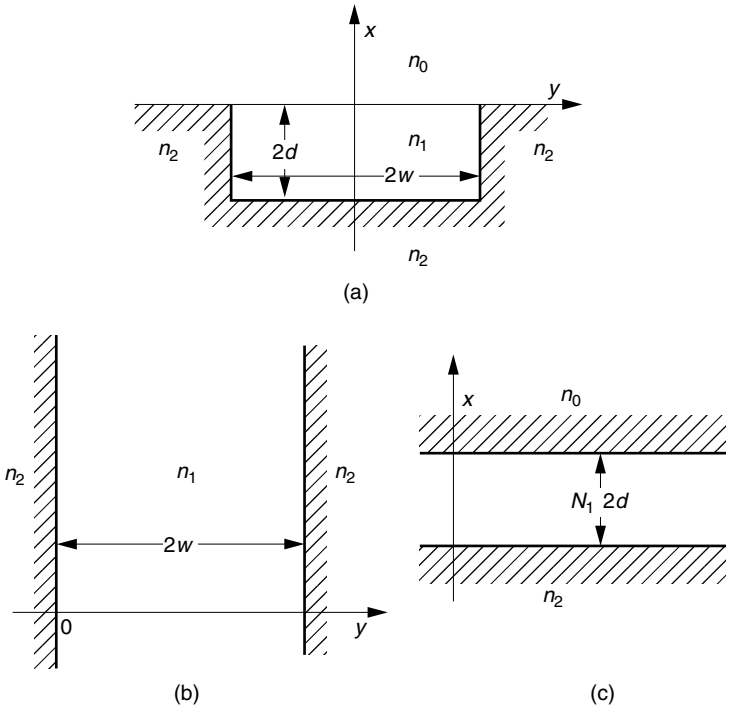


**Figure 10.6** Explanation of the effective index method.

**Step 2.** The effective index of refraction $N_1$ is used as the refractive index of the core layer of the slab optical guide shown in Fig. 10.6c, which is an asymmetric guide. The characteristic equation from Eq. (9.149) is

$$\frac{K\left(\dfrac{\gamma_0}{n_0'^2}+\dfrac{\gamma_2}{n_2'^2}\right)}{K^2-\dfrac{\gamma_0\gamma_2}{n_0'^2 n_2'^2}}=\tan 2Kd \tag{10.30}$$

where

$$\begin{aligned} n_0' &= \frac{n_0}{N_1} \\ n_2' &= \frac{n_2}{N_1} \end{aligned} \tag{10.31}$$

When $n_0$ is air and is much smaller than any other refractive index, Eq. (10.30) can be approximated in a manner similar to that mentioned in Example 9.6 and becomes

$$-\cot 2Kd=\frac{\gamma_2}{n_2'^2 K} \tag{10.32}$$

with

$$(Kd)^2+(\gamma_2 d)^2=V^2 \tag{10.33}$$

where

$$V = kd\sqrt{N_1^2 - n_2^2}$$

Let's say one of the solutions of Eqs. (10.32) and (10.33) is $K_x$; then the propagation constant $\beta_{wd}$ is finally, from Eq. (9.150),

$$\beta_{wd}^2 = (N_1 k)^2 - K_x^2 \tag{10.34}$$

$\beta_{wd}$ is the required propagation constant of the rectangular optical guide.

The results obtained by the effective index method are compared with those of the previous section. Inserting Eq. (10.29) into (10.34) gives

$$\beta_{wd} = \sqrt{(n_1 k)^2 - K_x^2 - K_y^2} \tag{10.35}$$

This expression is identical to Eq. (10.23). The difference, however, is that $K_y$ in Eq. (10.35) was obtained with $n_2' = n_2/N_1$, whereas $K_{y0}$ was obtained with $n_2' = n_2/n_1$. Further discussions about method approximations can be found in Refs. 6 and 7.

## 10.3 COUPLING BETWEEN RECTANGULAR GUIDES

The results with the slab guides can immediately be used for calculating the coupling between rectangular guides. The geometry shown in Fig. 10.7 is considered. This geometry was generated by slicing the five-layer slab guide, such as mentioned in Section 9.9, by a plane parallel to the $x$–$z$ plane with width $2w$. In order to make use of the results for the TM modes in Section 10.1.3, the $E_{pq}^x$ mode will be considered. If we follow the assumption made in Section 10.1.1 that the $x$ and $y$ components are mathematically separable, the propagation constant $\beta$ of the coupled rectangular guide can be obtained by combining $K_{1x\ \text{even}}$ and $K_{1x\ \text{odd}}$ of the coupled slab guide in the $x$ direction with the $K_{y0}$ of a symmetric guide in the $y$ direction.

Even though the values of $K_{1x\ \text{even}}$ and $K_{1x\ \text{odd}}$ obtained in Section 9.9.1 are immediately usable, the values of $K_{y0}$ have to be calculated using the characteristic equations (9.26) and (9.27) for the TM mode. Once these values are obtained, the required propagation constants are found as

$$\beta_{1e} = \sqrt{(n_1 k)^2 - (K_{1x\ \text{even}})^2 - K_{y0}^2} \tag{10.36}$$

$$\beta_{1o} = \sqrt{(n_1 k)^2 - (K_{1x\ \text{odd}})^2 - K_{y0}^2} \tag{10.37}$$

and the coupling length is

$$L = \frac{\pi}{\beta_{1e} - \beta_{1o}} \tag{10.38}$$

An actual calculation is demonstrated in the next example.

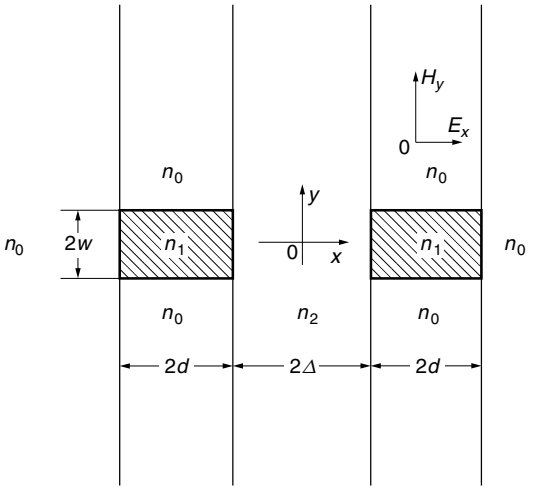


**Figure 10.7** Rectangular coupled guides.

**Example 10.2** Find the transfer length $L$ of the rectangular coupled guide with the dimensions and physical parameters shown in Fig. 10.8.

***Solution*** Simultaneous equations (9.26) and (9.27) have to be solved first. The same approach as in the previous example will be used. Set

$$f(K_y w) = n^2 K_y w \tan K_y w - \sqrt{V_0^2 - (K_y w)^2} \tag{10.39}$$

The function $f(K_y w)$ is plotted with respect to $K_y w$. The intersections of $f(K_y w)$ with the $K_y w$ axis are the solutions.

$$K_{y0} = 3.68903 \tag{10.40}$$

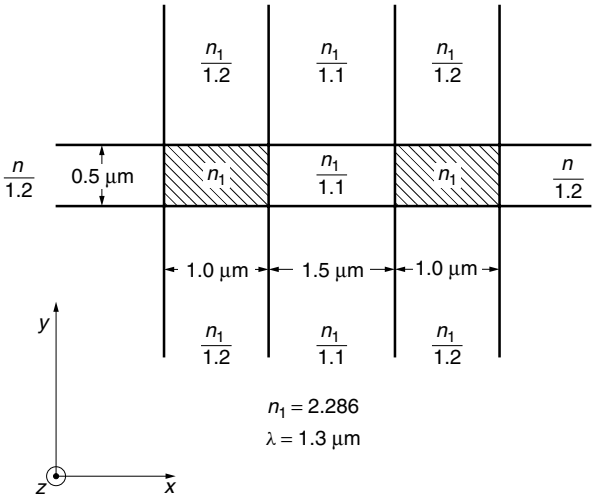


**Figure 10.8** Geometry and physical parameters of the rectangular coupled guide.

The progagation constants $\beta_{1e}$ and $\beta_{1o}$ are found by inserting Eqs. (9.201) and (10.40) into Eqs. (10.36) and (10.37).

$$\beta_{1e} = 10.13728\ \mu\text{m}^{-1}$$

$$\beta_{1o} = 10.13652\ \mu\text{m}^{-1}$$

The coupling length $L$ for the rectangular coupled guide is

$$L = \frac{\pi}{\beta_{1e} - \beta_{1o}} = 4.14\ \text{mm} \qquad \square$$

## 10.4 CONFLECTION

Reflection, refraction, and diffraction are words describing the change in the direction of light rays. The Latin verb *flectere* means "to bend" and *frangere* means "to break."

Di Francia [8] coined a new word — *conflection* — meaning the change in the direction of propagation at the joint of two cones of guiding layers.

When a light beam is launched into a uniform flat slab optical guide, it zigzags in the plane perpendicular to the boundary. However, in the plane parallel to the boundary, the light beam will no doubt propagate along a straight line because it is the fastest path to go from point $A$ to point $B$. This is Fermat's principle.

Would it still be the fastest path between $A$ and $B$ if the guide surface were bent, and if the light ray were not allowed to leave the surface? Let us conduct a small experiment. Draw a straight line $\overline{AB}$ in the center of a piece of cardboard as shown in Fig. 10.9a. Lay a piece of string over the line and attach the string to the cardboard at points $A$ and $B$. Fold the cardboard any way you wish with the string outside so that the string can be moved around but does not move off the surface, as shown in Fig. 10.9b. You will soon discover that no matter how you bend the cardboard, the string neither sags nor moves away from the pencil line $\overline{AB}$.

From this fact, one can find the path of light in a folded guide. The law of conflection is that the light path is bent such that the light path becomes a straight line when the bend is developed (unfolded) to be flat. This can be restated as saying that the incident angle $\theta_i$ with respect to the normal to the edge is the same as the transmitted angle $\theta_t$ as shown in Fig. 10.9c. This principle will be explained further by an example.

**Example 10.3** Find the light path when a light beam is launched into a tetrahedral (figure with four equivalent triangular faces) guide as shown in Fig. 10.10.

***Solution*** Let the light beam incident on the tetrahedron $abcd$ be parallel to the optical axis (dashed line), as shown in Fig. 10.10(1).

First, face $abc$ is folded in as $ab'c$ and a straight line $\overline{AB}$ is drawn in face $ab'c$, as in Fig. 10.10(2).

Face $ab'c$ is folded back to the original place $abc$. Now, face $bcd$ is unfolded so that $bcd'$ and $abc$ are in the same plane and the incident beam is further extended to $\overline{BC}$ as in Fig. 10.10(3).

Face $bcd'$ is folded back to the original position and then, this time, face $bcd$ is folded inside the tetrahedron until face $b'cd$ is pressed down onto the surface of the

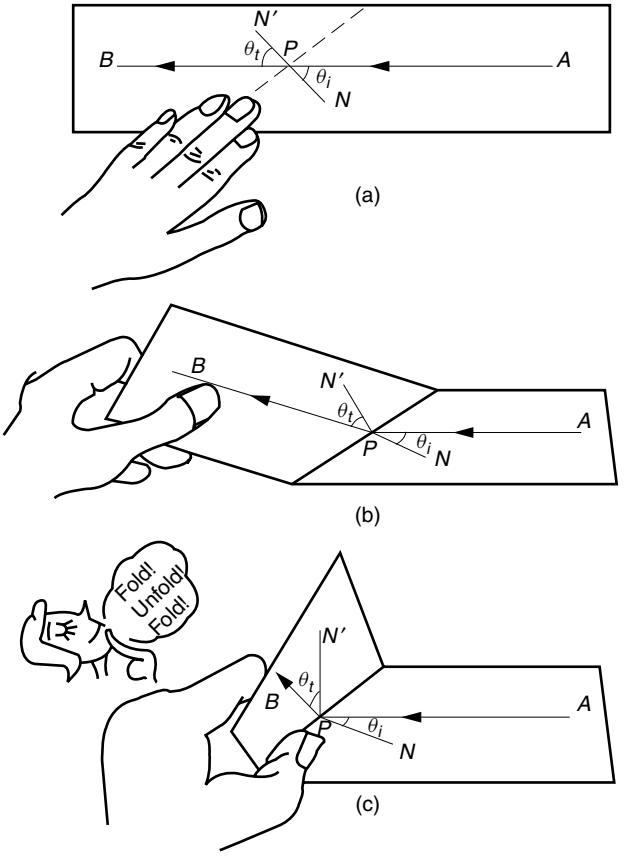


**Figure 10.9** Operation of FUF (fold–unfold–fold). (a) Developed (opened up to be flat). (b) Folded halfway. (c) Folded at 90°.

substrate. Then the line $\overline{BC}$ drawn on face $b'cd$ is extended onto the substrate to finally draw the emergent beam.

Figure 10.11 explains how to draw the same light path using the equality of the angles of incidence and transmission across the bend. The incident light beam is drawn at the far right-hand side of Fig. 10.11, and the faces of the tetrahedron that the beam encounters are drawn from right to left. Angles of incidence and transmission for points $A$, $B$, and $C$ are made equal, giving the light path shown.

A planar lens based on this principle is called a *conflection* lens. The conflection lens will be described as a practical example of the principle of conflection. □

### 10.4.1 Conflection Lens

Figure 10.12 shows a conflection lens [8]. A rectangular block with one of its ends shaped into a semicircular cylinder is placed on top of a larger block. It looks like the deck of a ship. The entire surface of the two-tier substrate block is covered by a thin film, which acts as the nonplanar guiding (core) layer. When light is launched in the lower deck, the light is guided in the core layer on the surface of the structure and

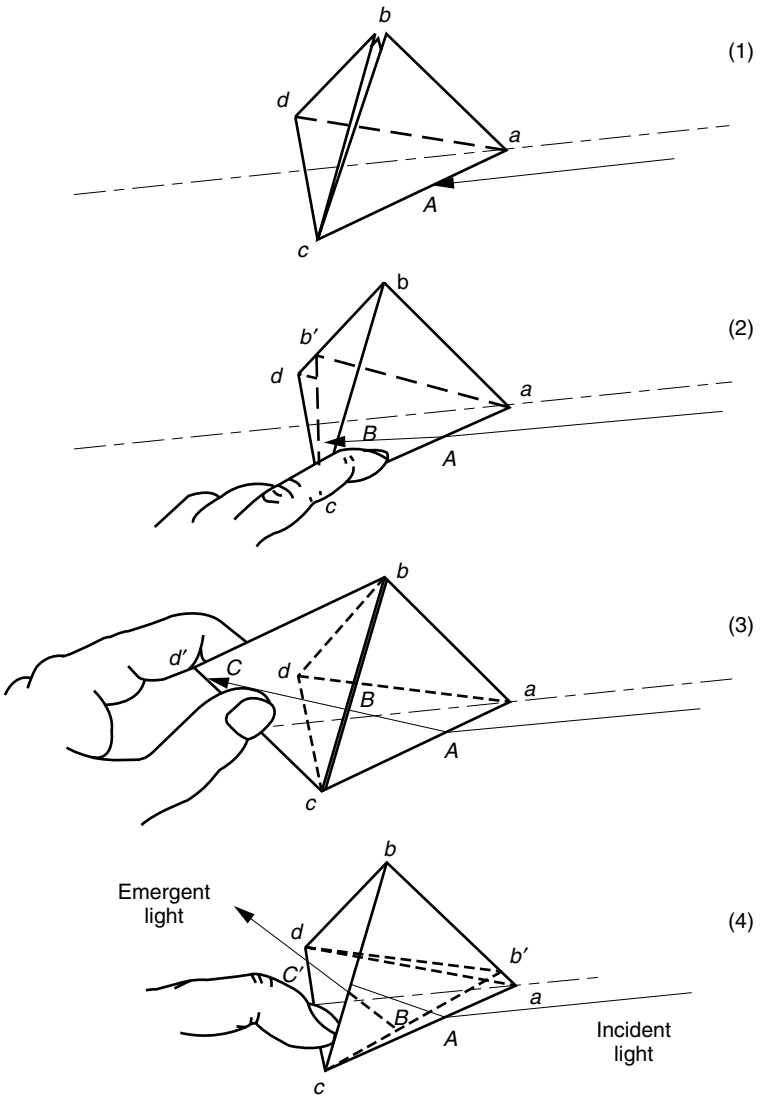


**Figure 10.10** Conflection by a tetrahedron.

eventually goes up to the upper deck. If a parallel beam is launched in the lower deck, the beam will be focused to a point on the upper deck because of the conflections taking place both at the foot and top of the short semicircular cylinder. The paths of three beams are shown in Fig. 10.12. The center beam that has entered on the optical axis keeps its direction parallel to the optical axis all the way. The beams on either side, however, change their directions at each conflection point, as shown in the figure. The three beams meet at the focal point on the upper deck.

The exact path of the light will be traced. Let the light beam $\overline{AB}$ be incident parallel to the optical axis. At the foot of the semicircular cylinder, conflection takes place. The path of light is determined by unfolding the folded small section of the side wall

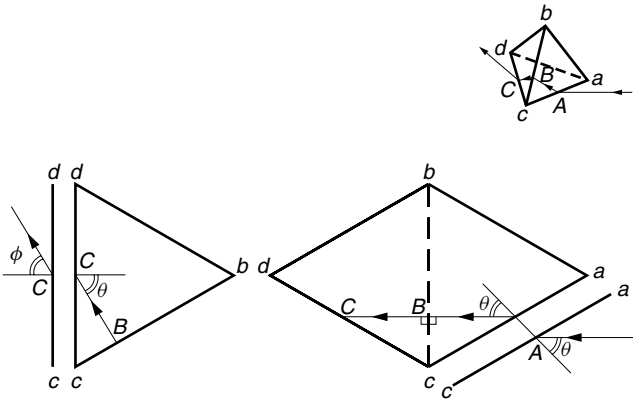


**Figure 10.11** Light path in the guide formed on the surface of a tetrahedral substrate. The law of conflection is used.

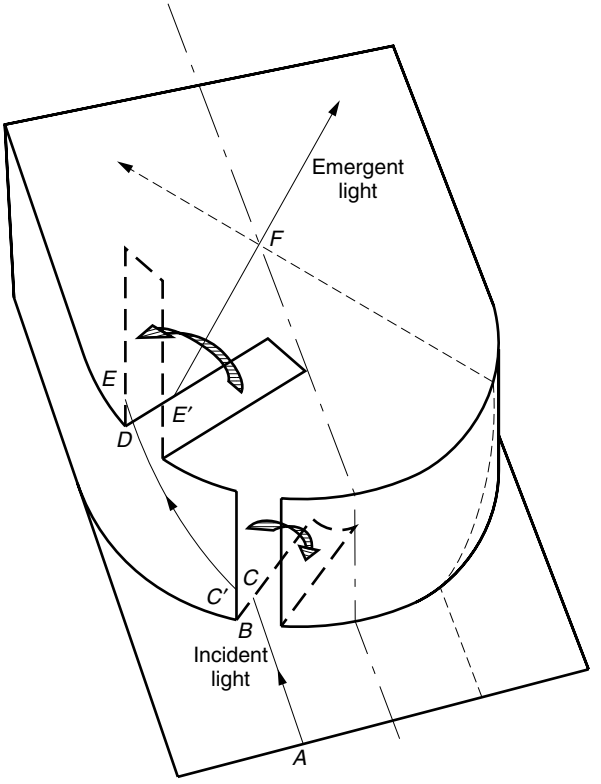


**Figure 10.12** Tracing the path of light of a conflection lens by the FUF law.

into the cylinder until it coincides with the plane of incidence. The path of light is a straight line $\overline{AC}$. The small unfolded section is then folded back to its original position. The curved wall is then unfolded to be flat, and the line $\overline{AC}$ is extended as the straight line $\overline{C'D}$.

At the edge made by the top plane and the side wall another conflection takes place. Unfold the top surface until it coincides with the plane of the cylinder wall, and draw the straight line $\overline{DE}$. Curve the cylinder wall back to its usual position and then fold the section back to the top surface. The extension $\overline{E'F}$ of $\overline{ED}$ is the emergent light path.

Figure 10.12 illustrates a conflection lens in which the incident and emergent beams are not in the same plane. The incident and emergent beams can be in the same plane by replacing the semicircular cylinder by a whole circular cylinder. Even though the idea of the conflection lens is interesting, scattering at the folded sections creates loss. Careful design of the surface is important to minimize the aberration of the lens.

## 10.5 VARIOUS KINDS OF RECTANGULAR OPTICAL WAVEGUIDES FOR INTEGRATED OPTICS

Representative structures of rectangular optical guides are summarized in Fig. 10.13. Each one is different. The choice has to be made from considerations such as connections with adjacent devices, difficulty of fabrication, loss in the guide, kinds of substrate materials to be used, and highest temperature allowable for fabrication if other devices are to share the same substrate with the optical guide. The types of rectangular guides shown in Fig. 10.13 are the following: ridge guide, rib guide, strip-loaded guide, embedded guide, immersed guide, bulge guide, metal guide, buffered metal guide, and photochromic flexible guide.

The various types of guides are explained below.

### 10.5.1 Ridge Guide

Figure 10.13a shows the structure of the ridge guide [9]. The normal difference in the refractive indices between the film and substrate is only a fraction of a percent, but if air is used as the covering medium, the difference in the refractive indices at the air–film interface is significantly larger and the evanescent wave is significantly reduced. Any roughness on the air–film interface upsets the guiding condition and creates radiation loss from the guide.

The core strip is deposited directly onto the substrate of a lower index of refraction. It looks structurally simple but strenuous efforts have to be made to ensure that the three side walls of the core strip are extra smooth to minimize the radiation loss.

### 10.5.2 Rib Guide

The rib guide shown in Fig. 10.13b is a film layer deposited on a substrate where the thickness of a strip along the center of the film is increased. Referring back to Fig. 9.6c, with an increase in the thickness of the guide, the angle $\theta_2$ of the direction of the component wave has to increase to match the boundary condition. The increase in $\theta_2$ means an increase in the effective index of refraction $N = n_1 \sin\theta_1$ in the center region of the film and the light is confined to this region.

This structure again has the core–air interface on three walls and stringent requirements on the smoothness of the surfaces have to be met.

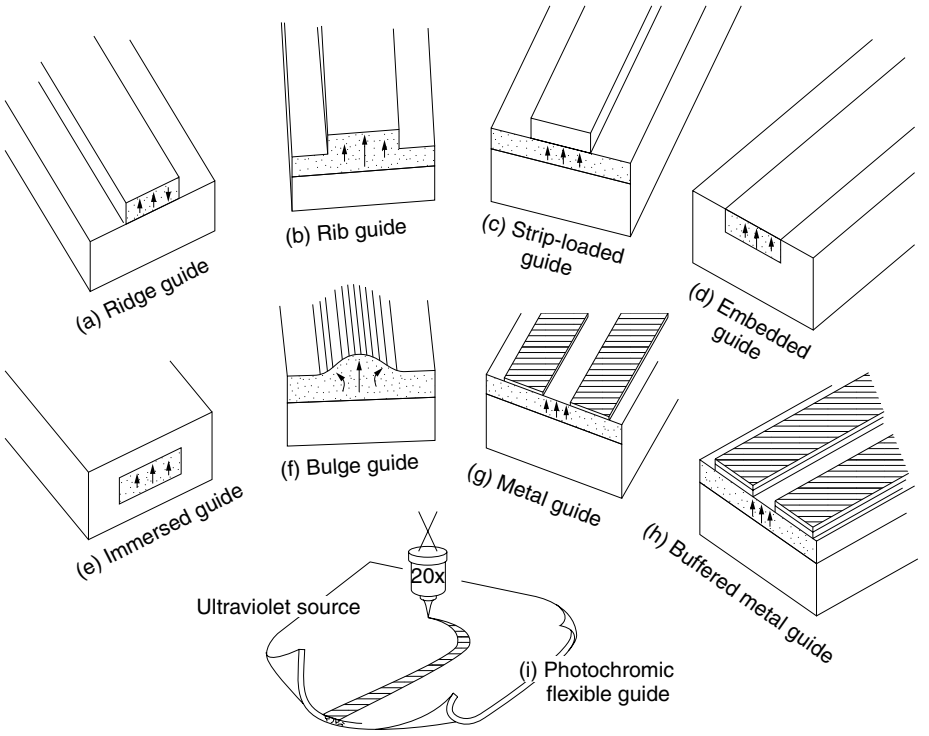


**Figure 10.13** Various kinds of rectangular guides. The field lines are the **E** field of the $E_{11}^{x}$ mode ($x$ is in the vertical direction).

### 10.5.3 Strip-Loaded Guide

A film is first deposited on a substrate of lower index of refraction. Then a strip whose index of refraction is lower than the film but higher than the covering to the film (e.g., air) is deposited on the film. This is the strip-loaded guide as shown in Fig. 10.13c. The principle of this guide can be explained by referring back to Fig. 9.4. In the region where the strip is deposited, the effective depth of the evanescent wave is deeper than that in the surrounding region and the angle $\theta_2$ of the direction of propagation of the component wave has to be increased. Therefore, the effective index of refraction $N$ is increased compared to that in the surrounding medium, and the light is confined to the region below the strip.

An advantage of this guide is that the stringent requirement of smooth surfaces at air–film interfaces is removed.

### 10.5.4 Embedded Guide

In the embedded or buried guide, only one of the surfaces is exposed to air, as shown in Fig. 10.13d, and the smooth surface requirement is not as demanding as the ridge or rib guide. When an electrooptic material is used for the core, the electrodes can be deposited in direct contact with the core so that the external field can be effectively applied. If two embedded guides are placed in close proximity so that the evanescent

fields overlap, then coupling can occur between the guides via the evanescent field. This is the basis of the optical guide coupler.

### 10.5.5 Immersed Guide

In the immersed guide, the core is completely immersed in the cladding medium, as shown in Fig. 10.13e. The mathematical analysis is simpler because of the symmetries in both the $x$ and $y$ directions. There is no cutoff of the dominant mode. This geometry, however, is not suitable for devices that need electrodes.

### 10.5.6 Bulge Guide

The bulge guide is a variation of the rib guide, as shown in Fig. 10.13f. The shape is not too critical but again the smoothness of the surface is important to minimize radiation loss. It possesses characteristics similar to the rib guide.

### 10.5.7 Metal Guide

The guiding film layer of this guide is covered by a pair of metal strips, as shown in Fig. 10.13g. In the section where the film is covered by the metal, the evanescent wave is removed and the effective height of the guide is reduced. In Fig. 9.6c, as the guide thickness decreases, $\theta_2$ decreases, and therefore so does the effective index of refraction $N$. The center region is bordered by regions of lower index of refraction, and a guide is formed.

Some loss of light power occurs on the metal surface because the metal is not a perfect conductor at optical frequencies. The complex refractive index of silver at optical frequencies is $\tilde{n}^2 = -16.32 - j0.5414$, and that of aluminium is $\tilde{n}^2 = -39.88 - j15.56$. The $\tilde{n}^2$ of a dielectric material like glass is a pure real number. The imaginary part of $\tilde{n}$ is associated with the conductivity of the metal and a larger number corresponds to a higher metal conductivity.

In a metal guide, the metal layers can conveniently be used as electrodes for applying an external control field for an electrooptic device. The electrooptic light modulator is an example of using such a feature.

### 10.5.8 Buffered Metal Guide

The light loss in the metal layer in the metal guide can be minimized by placing a thin dielectric buffer layer between the metal and film layers, as shown in Fig. 10.13h. The index of refraction of the buffer layer has to be lower than that of the film to confine the light primarily in the film layer. By adjusting the thickness of the buffer layer, the absorption for selected modes can be reduced. This property can be used as a mode filter. Since the thickness of the buffer layer is only a few tenths of a micrometer, the metal layer can still be used effectively for applying the external electric field for electrooptic devices.

### 10.5.9 Photochromic Flexible Guide

A photochromic material is a transparent material that changes to dark blue when it is exposed to ultraviolet light. Besides changing color, its index of refraction increases

for light wavelengths longer than the exposing ultraviolet light. This property of photochromics can be used to fabricate an optical guide [10].

A photochromic layer is deposited onto an acetate sheet or a glass substrate. Using an ultraviolet beam, an optical guide pattern is written onto the photochromic layer, as shown in Fig. 10.13i. Unlike other guides discussed in this section, the photochromic guide is flexible. The guide fades away in a few tens of minutes, which can be an advantage or disadvantage depending on the application. The film can be reactivated countless times with minimum fatigue.

## 10.6 POWER DIVIDERS

Figure 10.14 shows an example of a network of fiber-optic communication systems. It is evident that the simple Y junction power divider is a crucial component of such a network. Important considerations in designing the power divider are the following:

1. Accurate division of the input power into the prescribed proportions.
2. Minimum loss of light power in the divider.
3. Easy coupling to an external optical fiber circuit with minimum coupling loss.

### 10.6.1 The Y Junction and Arrayed-Waveguide Grating

The Y junction, although structurally very simple as shown in Fig. 10.15a, is nevertheless a very useful device. A practical difficulty in fabrication is the restriction on the angle $\theta$ between the output ports. It has to be less than $1^\circ$ if the branching loss is to be held below 1 dB. This restriction means the divider will be long if the output ports are to be sufficiently separated for coupling to an external circuit.

Multiport junctions can be fabricated by staggering the Y junction, as shown in Fig. 10.15b. The number of ports increases very rapidly by staggering the junctions. However, the insertion loss of the divider increases each time a new stage is added.

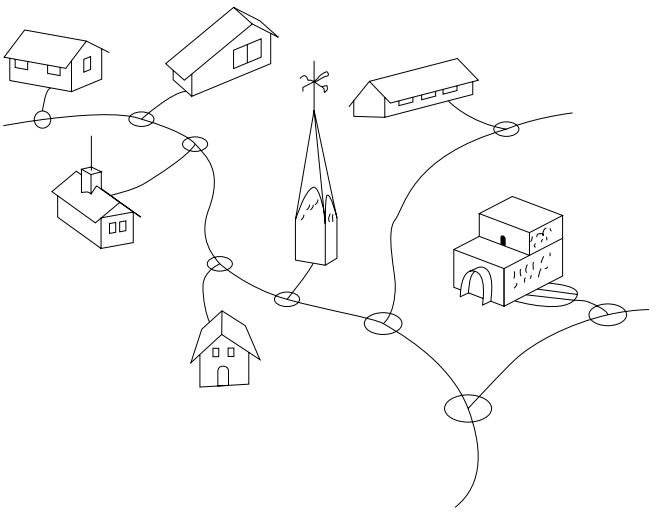

**Figure 10.14** Fiber-optic network connected by three-port power dividers.

The multimode interference (MMI) splitter shown in Fig. 10.15c aleviates the difficulties associated with concatenation of the Y junctions. The MMI splitter consists of a single-mode input port and several single-mode output ports with a multimode region in the middle section. The axes of the output ports are positioned to coincide with the maxima of the standing-wave pattern established in the multimode region.

The parameters can be designed for low loss as well as for a balanced division of power in the output ports [11,12].

Figure 10.15d shows the geometry of the arrayed-waveguide grating (AWG). This device sorts the closely spaced multi-wavelength light signals in the input waveguides into the output waveguides in accordance with the wavelength of the signal. It plays an important role in wavelength division multiplexing (WDM) of fiber-optic communcation systems [13,14].

$N$ input waveguides (typically $N = 8 \sim 128$) are connected to a slab optical guide, which forms a free space region of propagation. Light from any one of the input waveguides propagates across the free space region and illuminates the entrances of all the $M$ arrayed waveguides ($M$ is larger than $N$ and typically $M \doteqdot 2N$).

The arrayed waveguides as a whole act as a grating. The lengths of the arrayed waveguides are successively incremented with a step length of $\Delta L$. The exits of the $M$ arrayed guides are connected to another free space region. To the end of the free space region, $N$ output waveguides are connected.

The direction $\theta_{\text{out}}$ of the output beam is where constructive interference of the light emergent from the arrayed waveguides takes place. The condition for constructive

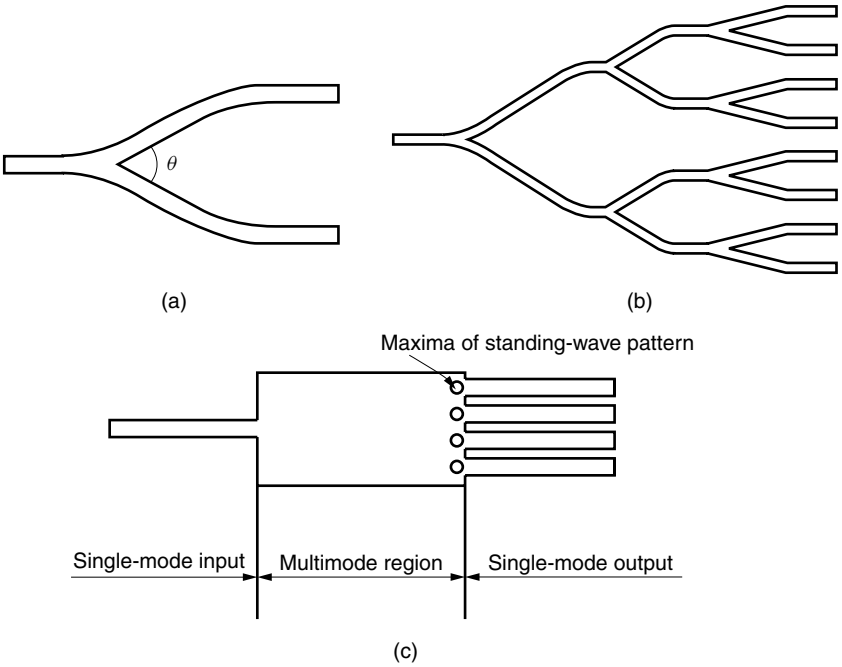


**Figure 10.15** Branching networks. (a) Y junction. (b) Eight-port branching circuit made of Y junctions. (c) Multimode interference (MMI) splitter. (d) Arrayed-waveguide grating (AWG). (e) Demultiplexing properties of an arrayed-waveguide grating. (After K. Okamoto and A. Sugita [16].)

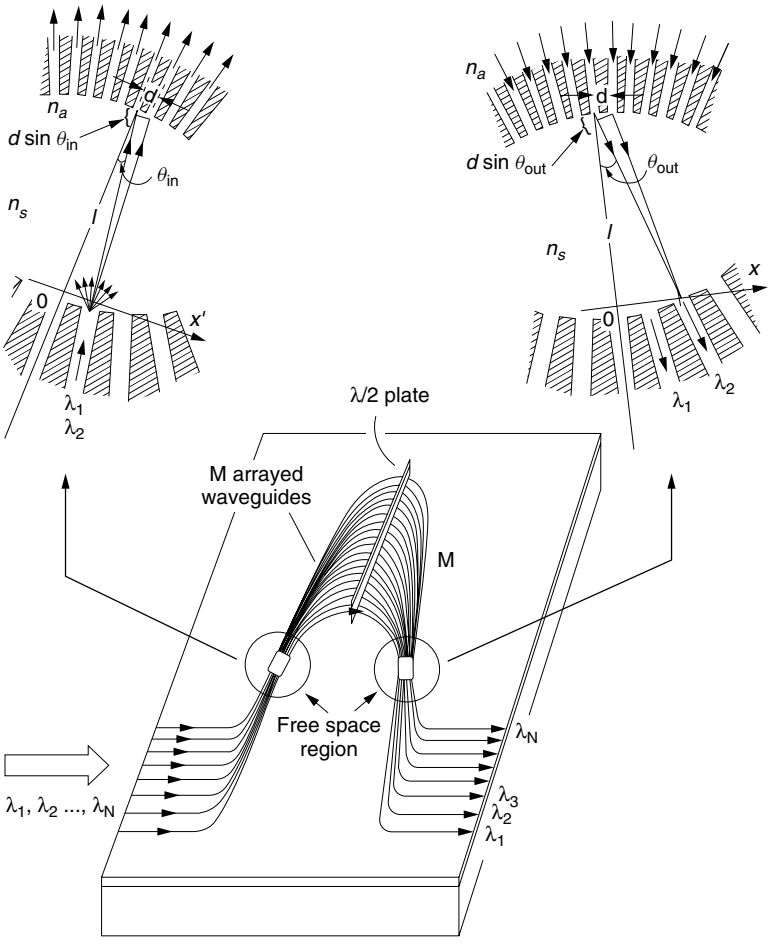


(d)

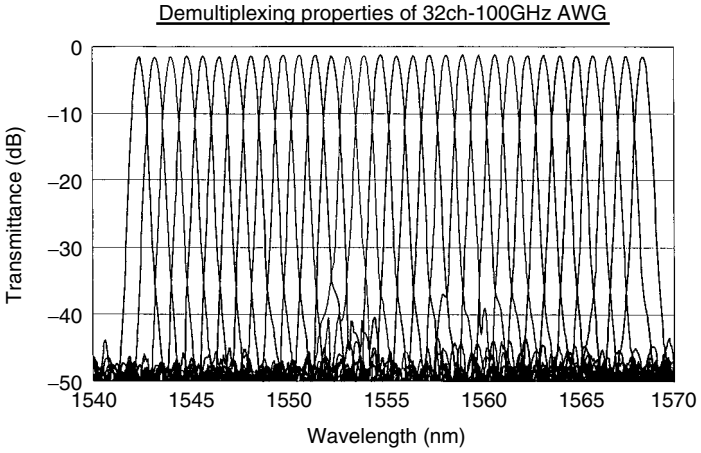


(e)

**Figure 10.15** (*Continued*)

At first glance, the Y junction might seem too inefficient a device for dividing the power into many subscribers, but in actual fact the number of output ports grows very rapidly. One only needs to stagger the Y junctions 20 stages to make enough ports to connect an entire city of one million households. An interesting analogy is that a sheet of newspaper can be divided into a million pieces by folding it only 20 times: $2^{20} = 1{,}048{,}576$.

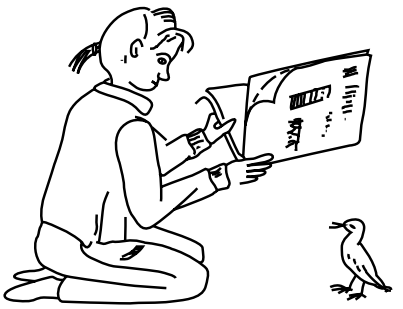

What is the least number of times you have to fold a sheet of newspaper to make a million pieces? Yes, it is only 20 times.

interference of the light with wavelength $\lambda$ originating from the input waveguide angle $\theta_{\text{in}}$ is

$$n_a \Delta L + n_s d(\sin\theta_{\text{in}} + \sin\theta_{\text{out}}) = p\lambda \tag{10.41}$$

where $n_a$ and $n_s$ are the refractive indices of the arrayed waveguides and the free space region, respectively. The arrayed waveguide spacing is $d$ and the diffraction order is $p$. Thus, from Eq. (10.41), $\theta_{\text{out}}$ for a given $\lambda$ and $\theta_{\text{in}}$ is found, and by manipulating the wavelength, the input signal at $\theta_{\text{in}}$ can be steered to any desired output waveguide $\theta_{\text{out}}$. This means that the AWG can perform an $N \times N$ matrix connection.

Next, the dispersion of the position of the output beam will be calculated. For small $\theta_{\text{out}}$

$$\sin\theta_{\text{out}} \doteqdot x/l \tag{10.42}$$

where $l$ is the length of the free space region. Form Eqs. (10.41) and (10.42),

$$\frac{dx}{d\lambda} = \frac{lp}{n_s d} \tag{10.43}$$

The value of the diffraction order $p$ is obtained from Eq. (10.41) for small $\theta_{\text{in}}$ and $\theta_{\text{out}}$ as $p = n_a \Delta L/\lambda$ and Eq. (10.43) becomes

$$\frac{dx}{d\lambda} = \frac{l n_a \Delta L}{n_s \lambda d} \tag{10.44}$$

Finally, the channel spacing of the AWG will be calculated. The diffraction pattern from an array of apertures of a finite number has already been calculated in Chapter 1. The result in Fig. 1.17 indicates that the first zero of an array with array width $c$ is situated at

$$f_x = 1/c \tag{10.45}$$

where $c$ is the array aperture.

This result is immediately applicable to our case by changing the physical parameters as

$$\begin{aligned} \lambda &\Rightarrow \lambda/n_s \\ c &\Rightarrow Md \\ f_x &\Rightarrow \frac{x}{\lambda l} n_s \end{aligned} \tag{10.46}$$

For simplicity $\theta_{\text{in}} = 0$ is assumed.

The value $x_W$ of the first zero of the radiation lobe in our case is

$$x_W = \frac{\lambda l}{M n_s d} \tag{10.47}$$

The quantity $2x_W$ is the "zero-crossing beam width" of the light peak at the entrance to the output waveguide.

If the channel wavelength spacing $\Delta\lambda$ is defined as the amount of change in the wavelength that shifts the peak to the first zero of the adjacent peak, namely,

$$\Delta x = x_W \tag{10.48}$$

where

$$\Delta x = \frac{dx}{d\lambda} \Delta\lambda \tag{10.49}$$

then from Eqs. (10.44), (10.47), (10.48), and (10.49) the channel spacing becomes

$$\Delta\lambda = \frac{\lambda^2}{n_a M \Delta L} \tag{10.50}$$

The channel wavelength spacing can be narrowed by increasing the number of the arrayed waveguides $M$ and the step length $\Delta L$.

The polyimide half-waveplate inserted in the midpoint of the arrayed waveguides acts as a TE–TM mode converter (Section 6.4.1) [15]. As seen from Eq. (10.41), the direction $\theta_{\text{out}}$ of the light peak depends on the effective index of refraction $n_a$, which is different for the TE and TM modes. The light in the TE mode (TM mode) that has travelled the first half of the arrayed waveguides travels in the TM mode (TE mode) in the second half of the arrayed waveguides. This averaging effect eliminates the polarization dependence of the AWG.

Figure 10.15e shows an example of the characteristics of the AWG [16]. In this example, the transmission of light is from one optical guide. The direction of transmission is from left to right and the device is used as a multiplexer, but the AWG is reciprocal and $\lambda_1, \lambda_2, \ldots, \lambda_N$ signals can be multiplexed into one optical waveguide.

### 10.6.2 Power Scrambler

Figure 10.16 shows an $8 \times 8$ scrambler made out of Y junctions. The power of any one input port is divided equally into the 8 output ports. Shown in Fig. 10.16a is an example of the division of inputs Ⓐ and Ⓔ into 8 output ports each of which has $A + E$. The flow of signal $A$ is indicated by the heavy lines and that of signal $E$ is indicated by the dashed lines. Each output has the same mixture of $A$ and $E$. Such a

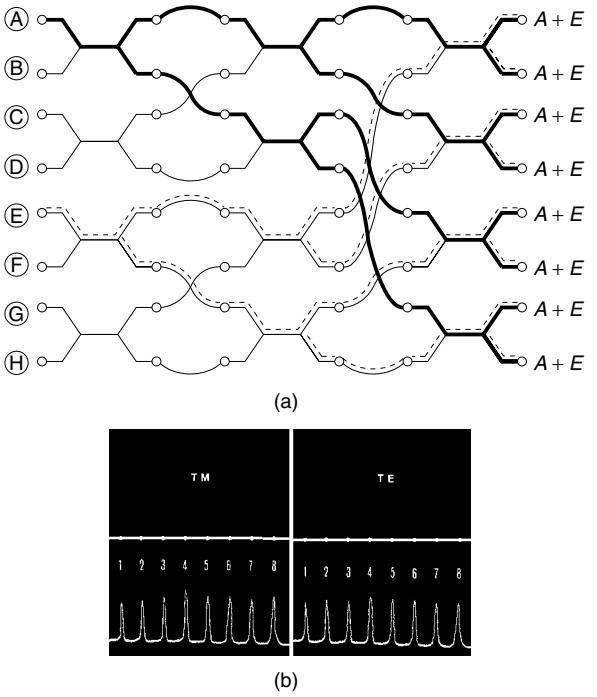


**Figure 10.16** An $8 \times 8$ star coupler. (a) Geometry of $8 \times 8$ star coupler. (b) Output from the first through eighth output ports when the first input port is illuminated. (After W. Doldissen et al. [17].)

scrambler, for instance, distributes 8 different TV channels to 8 subscribers, each of whom can receive 8 TV channels.

The connecting guides for such a geometry as shown in Fig. 10.16a cannot avoid crossing each other, but the crosstalk between the intersecting lines can be suppressed below $-23$ dB by choosing intersecting angles larger than $10^\circ$ [17].

Figure 10.16b shows the electrical output from the image made by an infrared vidicon camera.

A power scrambler such as the one shown in Fig. 10.16 is sometimes called a *star coupler* because of its configuration.

## 10.7 OPTICAL MAGIC T

Figure 10.17 shows the geometry of an optical magic T [18,19]. The function is quite similar to the magic T of microwave technology. Arms 1 and 2 are input arms and arms 3 and 4 are output arms. The dimensions of the input arms are identical, but those of the output arms are different. All arms are single-mode guides.

Figure 10.17a shows the field distribution when input arms 1 and 2 are equal in both amplitude and phase (symmetric feed). The distribution of the resultant field at the junction is double humped. Arm 3 is excited more than arm 4 because the shape of the resultant field at the junction conforms more with the $TM_0$ mode of arm 3 than with that of arm 4. The closer the shape of the illuminating light is to the amplitude distribution of the $TM_0$ mode, the higher the efficiency of excitation is because of the boundary condition of the continuity of the light.

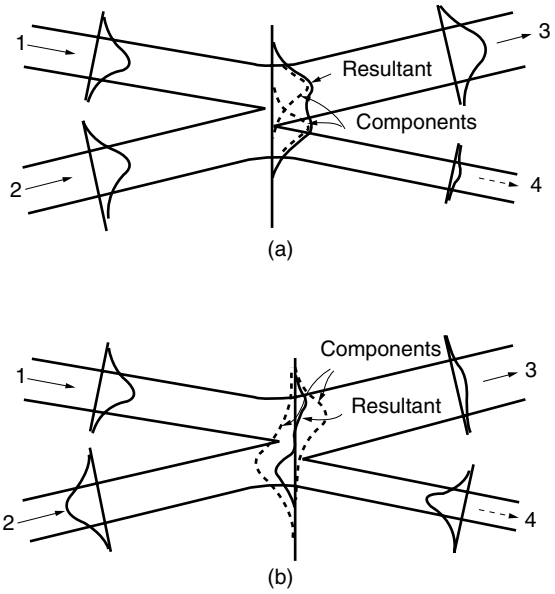


**Figure 10.17** Optical magic T. (a) Arms 1 and 2 are fed in phase. (b) Arms 1 and 2 are fed out of phase.

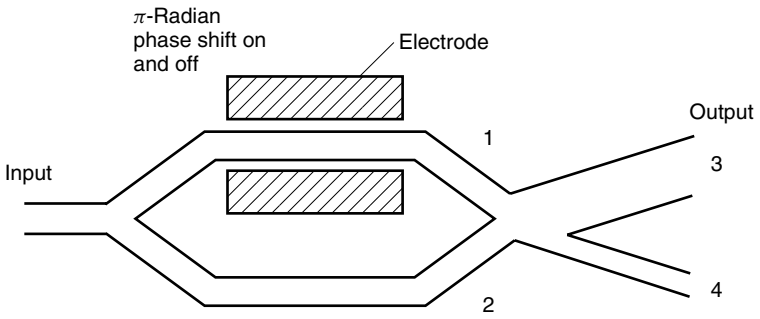


**Figure 10.18** Amplitude modulator using the magic T.

Figure 10.17b shows the field distribution when the input arms 1 and 2 are equal in amplitude but in opposite phase (antisymmetric feed). The distribution of the resultant field at the junction is antisymmetric in shape. Arm 4 is excited more than arm 3 because the field in the mouth of arm 3 is far from the shape of the $TM_0$ mode, whereas the shape of the resultant field at the mouth of arm 4 conforms with the fundamental mode in arm 4.

Neither symmetric nor antisymmetric feed will completely turn on or off the output arms; however, this device is still useful in applications that do not require complete switching. Figure 10.18 shows an example of the application of the magic T to an optical modulator. The modulator consists of the magic T and a Mach–Zehnder interferometer. The Mach–Zehnder interferometer is made of electrooptic material and the phase of one of the arms can be controlled by an external electric field. By

modulating the phase of the control arm between 0 and $\pi$ radians, each output light of arm 3 and 4 is amplitude modulated.

## 10.8 ELECTRODE STRUCTURES

In order to apply an external electric field to an electrooptic waveguide in the desired direction, the electrodes have to be properly designed. In this section, various electrode configurations are summarized. Configurations for bulk waves as well as for waveguides are included.

### 10.8.1 Laminated Electrodes

Electrodes are normally laminated by three metal layers, consisting of top, stopper, and contact layers. Figure 10.19 shows a cutout view of the lamination of an electrode (F. Saito, *private communication*).

1. The top layer is almost always gold because of the ease with which gold connecting wire is bonded to the electrode.
2. A chemical reaction would take place on the surface of some substrate materials if gold were in direct contact. GaAs is especially noted for reaction with gold. Metal for the contact layer (bottom layer) has to be chemically inactive and possess good affinity and low contact resistance to the surface of the substrate. Ti, Ni, Sn, Zn, and Cr are good candidates for this layer.

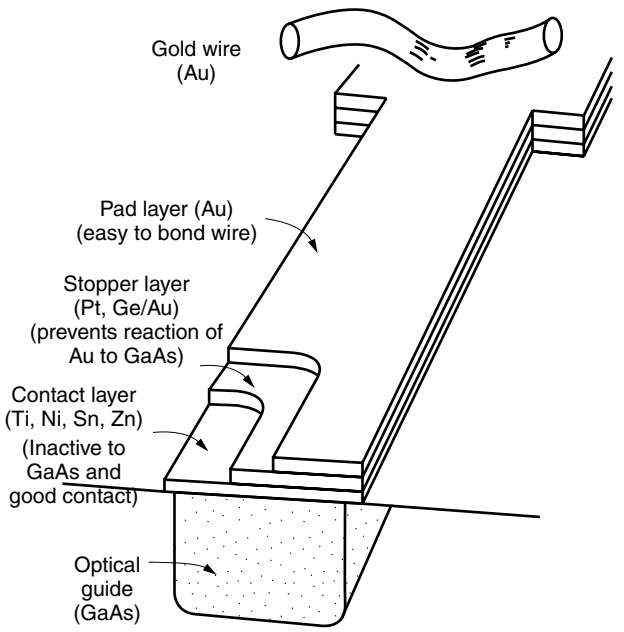


**Figure 10.19** Electrode lamination.

3. The stopper layer, which is the middle layer, has to completely shield both the contact layer and the surface of the substrate from chemical reaction with the top gold layer. The criteria for selecting the metal for the stopper layer are that the metal must have a high conductivity and a good affinity to both top and bottom metal layers. Pt and an alloy of Au and Ge satisfy these criteria and are most often used as the material for the stopper layer.

The most common combinations of metals for lamination are Au–Pt–Ti and Au–Ge/Au–Ni.

A single layer of Au or Al is often used as a temporary electrode in a laboratory. The Al, however, can be used only when low electrical current density is drawn from the electrode because of its poor electrical contact.

When a metal electrode is deposited directly over the surface of the guide, not only does the optical transmission loss increase, but the effective index of refraction of the optical guide decreases. These influences are larger for the TM mode. With the TM mode, the index of refraction decreases by $(1-2) \times 10^{-4}$ while with the TE mode, the decrease is one-fifth of this value [20].

A thin buffer layer ($\sim$0.3 μm), with an index of refraction lower than the core of the guide, is inserted between the electrode and the optical guide to solve the problem of the decrease in the index of refraction. Common buffer layer materials are $MgF_2$, $Al_2O_3$, and $SiO_2$.

Finally, an indium oxide ($In_2O_3$) or indium tin oxide (ITO) coating is used when the electrodes have to be transparent.

### 10.8.2 Electrode Configurations

Figure 10.20 illustrates various electrode configurations for applying external electric fields to electrooptic waveguides. Figures 10.20a and 10.20b are for bulk waves, where the light may propagate in the entire cross section of the crystal. The rest of the configurations are for guided waves, where the light propagates only inside the optical guide.

#### *10.8.2.1 Applying a Longitudinal Field to Bulk Waves*

Figure 10.20a shows the electrodes that provide an electric field parallel to the direction of light propagation. Transparent electrodes have to be used. As was pointed out in Example 5.2, the amount of change $\Delta\phi$ in the phase is determined by the applied voltage and is independent of the length of the crystal. This configuration requires a high voltage. With most crystals, the required control voltage is higher than several kilovolts to obtain $\Delta\phi = \pi$ radians of phase shift.

#### *10.8.2.2 Applying a Transverse Field to Bulk Waves*

In Fig. 10.20b, the direction of the external field is perpendicular to the direction of light propagation. This time, the amount of phase shift $\Delta\phi$ can be increased by choosing a longer crystal. However, the length of the crystal cannot be increased indefinitely if the external electric field $\varepsilon$ is modulated at a high frequency. At higher modulation frequencies, the transit time for the applied electric field $\varepsilon$ to travel from one end to the other end of the electrodes becomes important. For instance, the direction of the $\varepsilon$ field at one end can be opposite to that at the other end because of the long transit time,

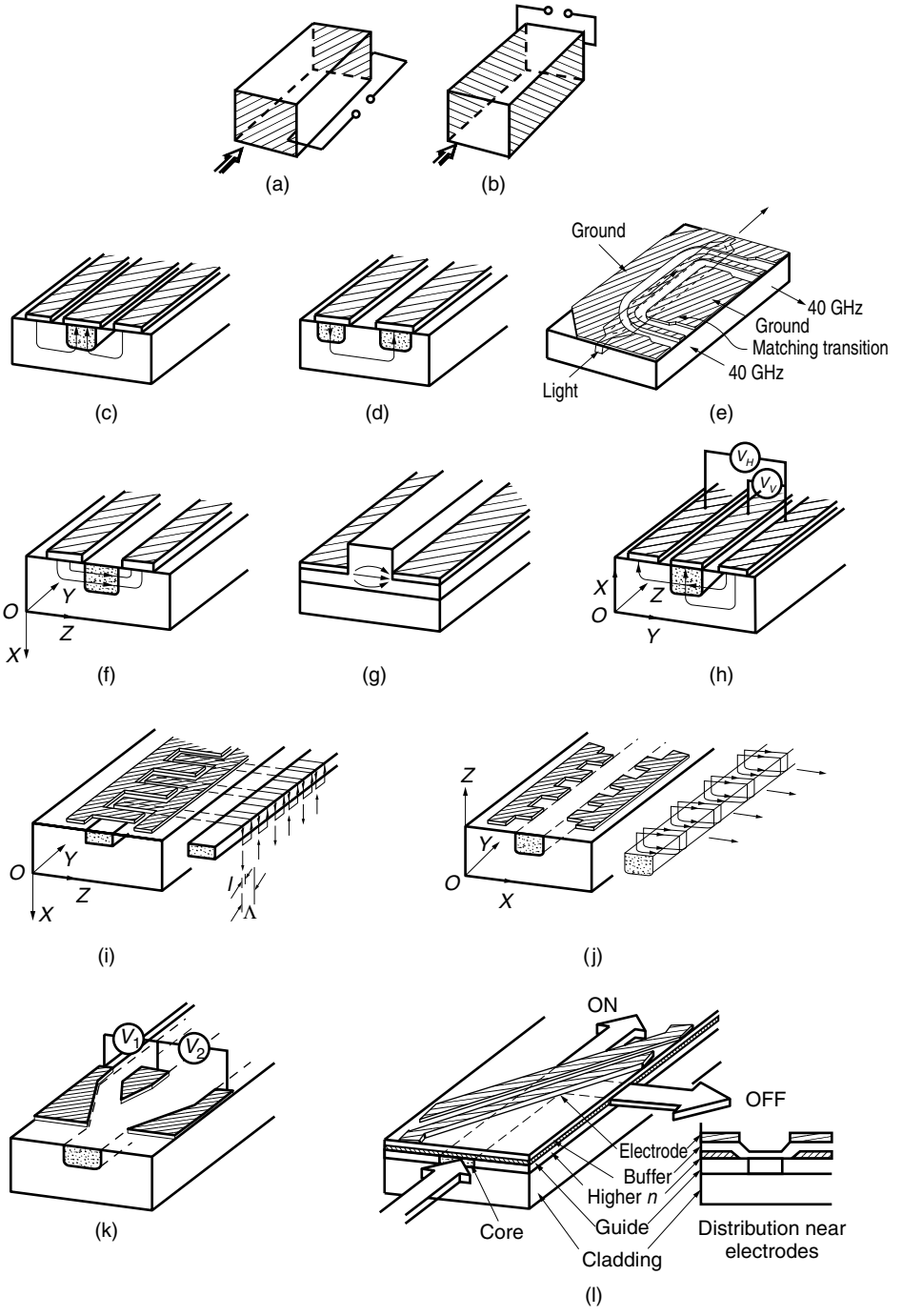


**Figure 10.20** Various electrode configurations on electrooptic waveguides. (a) Bulk longitudinal field. (b) Bulk transverse field. (c) Vertical field in an embedded guide. (d) Differential field. (e) Velocity matched Mach–Zehnder interferometer. (f) Horizontal field in an embedded guide. (g) Horizontal field in a rib guide. (h) Horizontal and vertical fields. (i) Periodic vertical field. (j) Periodic horizontal field. (k) Trimming electrodes. (l) Switching electrodes.

and the efficiency of modulation decreases. This, however, can be avoided by treating the electrodes as a pair of transmission lines, and designing the phase velocity of the modulating signal $\varepsilon$ to match with that of the light inside the crystal. In this way, the propagating light always sees the same $\varepsilon$ throughout transmission in the crystal. The electrodes should be terminated by a proper impedance so that there is no standing wave creating periodic zero fields and decreasing the efficiency.

All the electrodes in the following configurations are for guided waves.

#### 10.8.2.3 Vertical Field in an Embedded Guide

Figure 10.20c shows an electrode layout for applying a vertical field to an embedded guide. Since the electrical lines of force are always perpendicular to the surface of a conductor, the vertical field is obtained by depositing one electrode immediately above the optical guide, and the other electrode is split into two strips, one on each side of the center electrode.

In order to minimize the transmission loss and lowering of the effective index of refraction due to the direct contact of metal with the optical guide, a lower-refractive-index buffer layer has to be inserted. This is true with any of the electrodes for the vertical field, and as mentioned above, the necessity for the buffer layer is greater when the optical guide is excited by the TM mode.

#### 10.8.2.4 Vertical Field in Adjacent Embedded Guides

Figure 10.20d shows a pair of electrodes that provides a vertical electric field of opposite polarity to two adjacent embedded guides. The pair of electrodes is used to cause maximum imbalance between the effective indices of refraction of the two guides. The electric lines of force leave in a downward direction from one of the electrodes and return in an upward direction to the other electrode. The directions of the electric fields in the two optical guides are opposite; one creates $\Delta n$ while the other creates $-\Delta n$, and the maximum differential in the indices of refraction is achieved.

The Mach–Zehnder interferometer is an example of a device that often uses this electrode configuration. In a Mach–Zehnder interferometer, light traveling initially along a single path is split into two separate paths and then later recombined into a single path again. Any factor that affects the two separate paths differently will result in a change in the interference of the recombined light.

#### 10.8.2.5 Velocity Matched Mach–Zehnder Interferometer

A traveling-wave type modulator is shown in Fig. 10.20e [21]. A coplanar waveguide (two-dimensional coaxial cable) is deposited over the Mach–Zehnder optical interferometer substrate. The phase velocity of the microwave signal propagating along the coplanar waveguide is matched with that of the light in the Mach–Zehnder interferometer.

As mentioned in Section 10.8.2.2, the synchronization of these two velocities achieves not only a high modulation efficiency but also a wideband frequency modulation.

#### 10.8.2.6 Horizontal Field in an Embedded Guide

An electrode arrangement that can provide a horizontal (parallel to the top surface of the guide) electric field inside an embedded guide is shown in Fig. 10.20f. The electric lines of force are almost horizontal but there is always some deviation from

a truly horizontal field. A buffer layer is not needed because the electrodes are not in direct contact with the surface of the guide. The maximum voltage that can be applied between the electrodes is limited by either the arc breakdown voltage between the electrodes (See Problem 10.5) or crystal damage.

#### 10.8.2.7 Horizontal Field in a Rib Guide

Figure 10.20g shows the electrodes for applying a horizontal electric field to a rib optical guide. Compared to Fig. 10.20f, the configuration in Fig. 10.20g has a higher upper limit on the applied voltage, a more closely horizontal electric field distribution, and less field divergence, but the configuration is applicable only to a rib guide.

#### 10.8.2.8 Horizontal and Vertical Fields

When more than a few elements of the matrix of the Pockels constants are used, applied fields may be required in both the horizontal and vertical directions. Figure 10.20h shows three electrodes that provide both vertical and horizontal fields simultaneously and yet each can be controlled independently to make sophisticated use of the properties of the crystal anisotropy.

#### 10.8.2.9 Periodic Vertical Field

Figure 10.20i shows the finger electrodes that provide periodic electric fields along the path of light propagation. Electric lines of force start perpendicularly to the surface of a tooth and terminate similarly at the adjacent tooth. The lines of force around the optical guide are shown in the side view of the figure indicating the direction of polarization of the applied electric field.

Such finger electrodes are used in a mode converter [22], a device that converts a TM mode to a TE mode or vice versa. The performance of the converter is very much wavelength dependent and the output is present only around the narrowly designed wavelength. Because of this property, the same device is also used as a wavelength filter.

The fundamental TM mode is vertically polarized, and the fundamental TE mode is horizontally polarized. Hence, the function of the TM to TE mode converter is to convert from vertical to horizontal polarization. Examples 7.13 and 10.4 provide the design details for such a mode converter.

In order to achieve a high efficiency of conversion, the tooth pattern has to be repeated. The maximum conversion is achieved when many teeth are arranged with a period such that the TE wave generated from each tooth adds up in phase at the exit of the converter.

#### 10.8.2.10 Periodic Horizontal Field

Another type of finger electrode pattern is shown in Fig. 10.20j. These electrodes provide periodic electric fields, but in the horizontal direction. At each region where the distance between opposing teeth is the shortest, horizontal electric lines of force are set up. These finger electrodes are also used for mode converters and wavelength filters based on the same principle as described for the periodic vertical field device. As mentioned earlier, the advantage of the horizontal field electrodes is that the electrodes are not in contact with the surface of the guide, and the transmission loss is small.

#### 10.8.2.11 Trimming Electrodes

In Fig. 10.20k, trimming electrodes have been placed at the location where one guide branches into two separate guides. In applications where splitting the light into the

two branch guides has to meet exact specifications, fabrication tolerances can be relaxed significantly if there is a provision for electronic tuning. For instance, in a Mach–Zehnder modulator, the amplitudes of the input to the two arms have to be exactly the same in order to achieve l00% modulation. Without electronic tuning, fabrication tolerance is severe. However, with the use of trimming electrodes, small fabrication faults can be corrected electronically. An imbalance in the applied voltages to the electrodes causes a small imbalance in the division of the light power into the two arms to correct for imperfect fabrication.

The earlier example of Fig. 10.20h gave an electrode configuration for applying horizontal and vertical fields. For some applications, one of the applied fields is used as the primary field, while the other is used in a trimming capacity.

#### *10.8.2.12 Switching Electrodes*

A pair of electrodes such as shown in Fig. 10.20l is used for switching the optical beam in a slab guide [23]. The switching action is based on total internal reflection. The index of refraction in the region between the electrodes is decreased by applying an external electric field so that total internal reflection takes place.

Realizable decreases in the index of refraction are small, which means that the critical angle is necessarily close to 90° so that the reflected and transmitted beams will be quite close to one another. In order to alleviate this problem, the effective index of refraction of the core slab is raised everywhere except in the region between the electrodes. This is done by first depositing a higher-index medium such as GaAs over the core, except at the location between the electrodes. In the region between the electrodes where no higher-index material was deposited, the effective index of the core dips. When an external field is applied, the dip deepens, total internal reflection takes place, and the beam is switched to the off axis.

## 10.9 MODE CONVERTER

Mode converters are used to convert a TM mode to a TE mode or vice versa. The Poincaré sphere interpretation of the operation of a mode converter was given in Example 7.13. In the mode converter example below, parameters for optimum conversion are explored using the indicatrix.

**Example 10.4** A TE $\leftrightarrow$ TM converter is fabricated, using the configuration shown in Fig. 10.20i. A lithium niobate slab with its crystal axis in the $Z$ direction is used.

(a) Find the cross-sectional ellipse of the indicatrix in the region where an $X$-directed electric field is applied by a pair of fingers.
(b) Consider a single pair of finger electrodes of length $l$, and let a vertically polarized TM mode be incident. Find the expression for the horizontally polarized TE mode at the exit of the finger electrode region.
(c) What is the spacing $\Lambda$ between the adjacent fingers for the optimum conversion?

***Solution***

(a) The material is $LiNbO_3$ and Eq. (5.10) applies. Since light propagates in the $Y$ direction, the "cross-sectional ellipse" of the indicatrix is obtained from Eq. (5.4) with

$y = 0$ and Eq. (5.10):

$$\frac{X^2}{n_o^2} + \frac{Z^2}{n_e^2} + 2r_{51}\varepsilon_x XZ = 1 \tag{10.51}$$

Equation (10.51) represents an ellipse rotated due to $\varepsilon_x$ and the angle $\theta$ of the rotation is obtained immediately from Eq. (5.35):

$$\theta = \frac{1}{2}\tan^{-1}\left(\frac{2r_{51}\varepsilon_x}{1/n_0^2 - 1/n_e^2}\right) \tag{10.52}$$

The lengths of the major and minor axes of the ellipse are represented in the rotated coordinates by

$$\frac{x'^2}{(N - \Delta N)^2} + \frac{z'^2}{(N + \Delta N)^2} = 1 \tag{10.53}$$

where

$$\begin{aligned} \Delta N &= \frac{1}{2}N^3\sqrt{B^2 + d^2} \\ \frac{1}{N^2} &= \frac{1}{2}\left(\frac{1}{n_o^2} + \frac{1}{n_e^2}\right) \\ d &= \frac{1}{2}\left(\frac{1}{n_o^2} - \frac{1}{n_e^2}\right) \\ B &= r_{51}\varepsilon_x \end{aligned} \tag{10.54}$$

(b) Since the cross-sectional ellipse is rotated by $\theta$, the allowed directions of polarization are at $\theta$ and $\theta + \pi/2$. It is this rotation that is used for the mode conversion. First, the amplitude $E_{\mathrm{TM}}$ of the incident vertically polarized TM mode is decomposed into the $\theta$ and $\theta + \pi/2$ directions and then each of these components propagates for the length $l$ of a finger. At the exit of the finger, the horizontal components of each of the allowed polarizations are found and combined to give the desired field. Referring to Fig. 10.21a the components in the $\theta$ and $\theta + \pi/2$ directions are

$$E_{X'} = E_{\mathrm{TM}}\sin\theta \quad \text{in the } X' \text{ direction}$$

$$E_{Z'} = E_{\mathrm{TM}}\cos\theta \quad \text{in the } Z' \text{ direction}$$

After each wave propagates a length $l$, $E_{X'}$ and $E_{Z'}$ become

$$E_{X'} = E_{\mathrm{TM}}\sin\theta\ e^{j(N-\Delta N)kl}$$

$$E_{Z'} = E_{\mathrm{TM}}\cos\theta\ e^{j(N+\Delta N)kl}$$

The resultant horizontal component $E_{\mathrm{TE}}$ becomes

$$\begin{aligned} E_{\mathrm{TE}} &= E_{\mathrm{TM}}\left(e^{j(N-\Delta N)kl} - e^{j(N+\Delta N)kl}\right)\sin\theta\cos\theta \\ &= -jE_{\mathrm{TM}}e^{jNkl}\sin(\Delta N \cdot kl)\sin 2\theta \\ E_{\mathrm{TE}} &= \mu E_{\mathrm{TM}} \end{aligned} \tag{10.55}$$

where

$$\mu = -je^{jNkl}\sin(\Delta N \cdot kl)\sin 2\theta \tag{10.56}$$

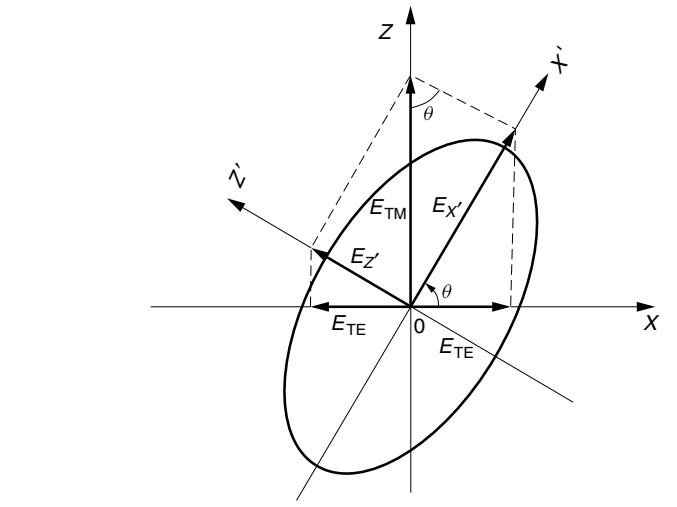


(a)

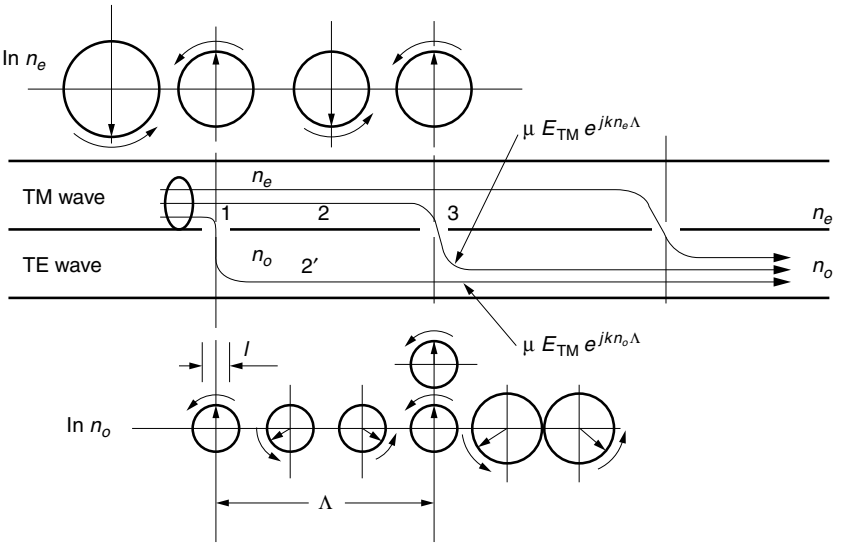


(b)

**Figure 10.21** Mode converter principle. (a) Rotation of the elliptical cross section of the indicatrix due to $\varepsilon_x$. (b) Coupling from the TM wave to the TE wave.

Thus, $\mu$ is the quantity associated with the amount of conversion in one finger pair. It increases with $l$ (as long as $\Delta Nkl < \pi/2$), and it increases as $\theta$ approaches $\pi/4$ rad.

(c) The optimum spacing $\Lambda$ between the fingers will now be found. For the sake of simplicity, let us assume that the length $l$ is much shorter than the spacing $\Lambda$ and let us use the fictitious model shown in Fig. 10.21b for explanation. Two guides are coupled through a series of holes; the TM wave is incident in the top guide and the TE mode is

generated in the bottom guide, even though in reality both propagate in the same guide. Each hole represents a finger electrode pair. The TM and TE modes see a different index of refraction. If the angle of the zigzag propagation in the guide is very small (or the fundamental mode is far away from the cutoff), the propagation constant of the TM mode is approximately $n_e k$ and that of the TE mode is $n_0 k$ in the region with $\varepsilon_x = 0$. The next question is how to maximize the emergent TE wave, which is the sum of all the waves leaked from the coupling holes (fingers). Since the propagation constants of the TM and TE modes are different, the phases of the contributing waves depend on which hole they have come from, and the spacings between the holes.

Compare the phase of the leaked component of the TE mode that leaked at hole 1 and took the route of $2'$ to reach hole 3, with the phase of the component of the TE mode that leaked at hole 3 and joined the TE mode. Taking into account the difference in the propagation constants in the upper and lower guides, the TE component taking the path of $1{-}2'{-}3$ is

$$\mu \mathrm{TE}_{\mathrm{TM}} e^{jkn_0\Lambda}$$

while that taking the path $1{-}2{-}3$ is

$$\mu \mathrm{TE}_{\mathrm{TM}} e^{jkn_e\Lambda}$$

The spacing $\Lambda$ of the holes that makes these two waves in phase is

$$k(n_o - n_e)\Lambda = 2\pi \tag{10.57}$$

With this choice of the spacing $\Lambda$, the outputs from the $N$ holes will add most efficiently, increasing the output $N$ times.

For $\lambda = 1.3$ μm and $LiNbO_3$, the optimum spacing is

$$\Lambda = 15.1 \text{ μm} \tag{10.58}$$

If this condition is satisfied, the amplitude of the TE wave from $N$ holes becomes

$$E_{\mathrm{TE}} = \mu N E_{\mathrm{TM}} \tag{10.59}$$

□

## PROBLEMS

**10.1** Find the number of possible modes of the ridge guide shown in Fig. P10.1. The TM-like mode is excited with physical parameters

$$n_1 = 1.55, \quad n_2 = 1.54, \quad 2d = 5.7 \text{ μm}, \quad 2w = 6.0 \text{ μm}, \quad \lambda = 1.3 \text{ μm}$$

**10.2** A slab optical guide with a cone-shaped indentation such as shown in Fig. P10.2 was illuminated by a parallel beam. What is the direction of the emergent beam? For what can such a guide be used?

**10.3** Two cone-shaped indentations are connected by their tips as shown in Fig. P10.3. For what can such a slab optical guide be used?

**10.4** An optical guide was formed on the surface of tetrahedron, *abcd*. The tetrahedron is placed such that the bisect of the bottom face is along the optical axis. The

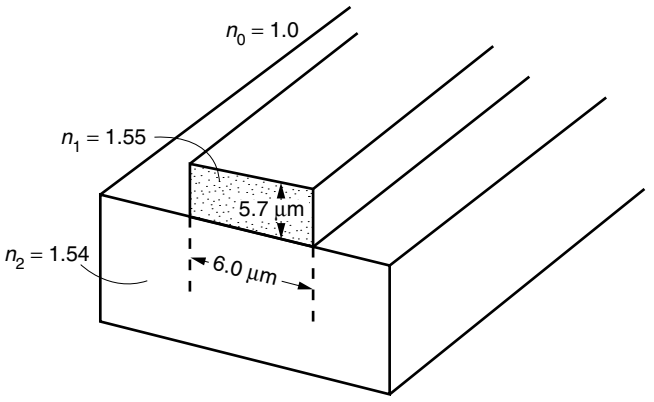


**Figure P10.1** Geometry of a ridge guide.

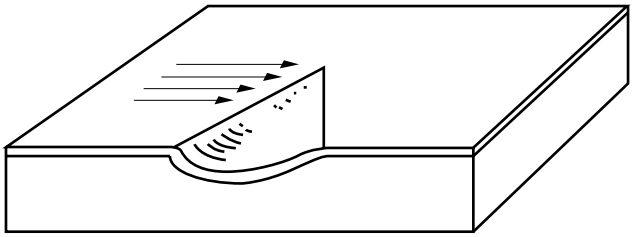

**Figure P10.2** A slab optical guide with cone-shaped indentation.

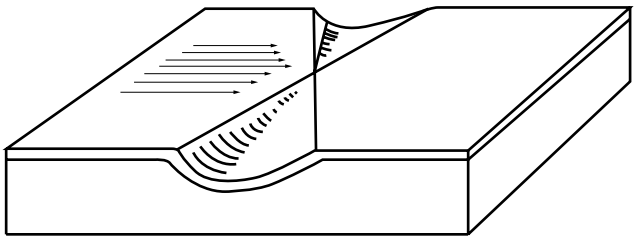

**Figure P10.3** A slab optical guide with double cone-shaped indentations.

light path on the surface of the tetrahedron looks like $ABC$ as indicated in Fig. P10.4. Find the location $A$ (length $aA$) such that the point $C$ of exit is at $dC = 2$ cm. The length of the edge of the tetrahedron is l0 cm. The incident light is parallel to the optical axis.

**10.5** The arc breakdown voltage is 30 kV/cm or 3 V/$\mu$m in air. What is the breakdown-voltage-limited phase shift $\Delta\phi$ obtainable by a phase shifter such as shown in Fig. 10.20f? The phase shifter is made of X-cut lithium niobate, and the horizontally polarized TE mode is excited with free-space wavelength $\lambda = 1.3$ μm. The length in the $Y$ direction is 1 mm.

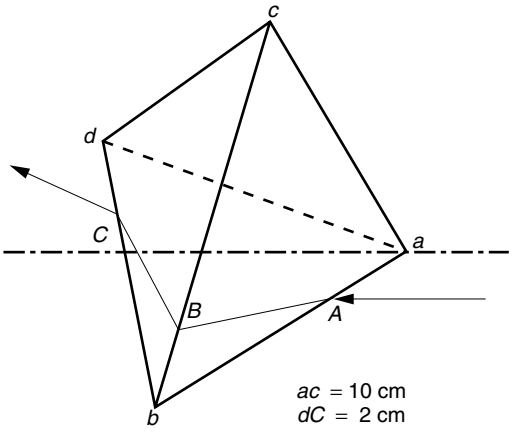


**Figure P10.4** Path of conflection.

## REFERENCES

1. T. Tamir (Ed.), *Guided-Wave Optoelectronics*, Springer-Verlag, Berlin, 1990.
2. R. G. Hunsperger, *Integrated Optics: Theory and Technology*, 4th ed., Springer-Verlag, Berlin, 1995.
3. A. R. Mickelson, *Guided Wave Optics*, Van Nostrand Reinhold, New York, 1992.
4. Y. Mushiake and M. Kudo, "Multilayered optical slab guide," in *Optical Guided-Wave Electronics*, by the Editorial Committee of the Special Project Research on Optical Guided-Wave Electronics of Japan, Tokyo, 1981, pp. 17–37.
5. E. A. J. Marcatili, "Dielectric rectangular waveguide and directional coupler for integrated optics," *Bell Syst. Tech. J.* **48**(7), 2071–2102 (1969).
6. K. S. Chiang, "Effective-index analysis of optical waveguides," *Proc. SPIE* **2399**, 2–12 (1995).
7. K. S. Chiang, "Analysis of rectangular dielectric waveguides: effective-index method with built-in perturbation correction," *Electron. Lett.* **28**(4), 388–390 (1992).
8. G. T. di Francia, "Conflection doublets," *J. Opt. Soc. Am.* **45**(8), 621–624 (1955).
9. H. P. Zappe, *Introduction to Semiconductor Integrated Optics*, Artech House, Boston, 1995.
10. A. G. Hallam, I. Bennion, and W. J. Stewart, "Photochromic stripe waveguide for integrated optics," in *First European Conference on Integrated Optics*, Oct. 14–15, pp. 26–28, 1981.
11. J. A. Besley, J. D. Love, and W. Langer, "A multimode planar power splitter," *J. Light wave Technol.* **16**(4), 678–684 (1998).
12. J. Leuthold and C. H. Joyner, "Multimode interference couplers with tunable power splitting ratios," *J. Lightwave Technol.* **19**(5), 700–707 (2001).
13. A. E. White, "Wavelength division multiplexing (WDM) has arrived. Critical to future system developments are integrated optical components fabricated using silicon optical bench technology," *Optics and Photonics News*, 27–30, March 2000.
14. H. Takahashi, S. Suzuki, K. Kato, and I. Nishi, "Arrayed-waveguide grating for wavelength division multi/demultiplexer with nanometre resolution," *Elec. Lett.* **26**(2), 87–88 (1990).
15. Y. Inoue, H. Takahashi, S. Ando, T. Sawada, A. Himeno, and M. Kawachi, "Elimination of polarization sensitivity in silica-based wavelength division multiplexer using a polyimide half waveplate," *J. Lightwave Tech.* **15**(10), 1947–1957 (1997).

16. K. Okamoto and A. Sugita, "Flat spectral response arrayed-waveguide grating multiplexer with parabolic waveguide horns," *Electron. Lett.* **32**(18), 1661–1662 (1996).
17. W. Döldissen, H. Heidrich, D. Hoffmann, H. Ahlers, A. Döhler, and M. Klug, "Integrated optical 8 × 8 scrambler in integrated optics," in *Proceedings of the 3rd European Conference ECIO 1985*, May 6–8, Berlin, Germany, pp. 225–228, 1985.
18. M. Izutsu, A. Enokihara, and T. Sueta, "Optical-waveguide hybrid coupler," *Opt. Lett.* **7**(11), 549–551 (Nov. 1982).
19. P. Sewell, T. M. Benson, T. Anada, and P. C. Kendall, "Bi-oblique propagation analysis of symmetric and asymmetric Y-junctions," *J. Lightwave Technol.* **15**(4), 688–696 (1997).
20. M. Masuda and J. Koyama, "Effects of a buffer layer on TM modes in a metal-clad optical waveguide using Ti-diffused $LiNbO_3$ C-plate," *Appl. Opt.* **16**(11), 2994–3000 (1977).
21. W. K. Burns, M. M. Howerton, R. P. Moeller, R. Krähenbühl, R. W. McElhanon, and A. S. Greenblatt, "Low drive voltage, broad-band $LiNbO_3$ modulators with and without etched ridges," *J. Lightwave Tech.* **17**(12), 2551–2555 (1999).
22. R. C. Alferness, "Electrooptic guided-wave device for general polarization transforms," *IEEE J. Quantum Electron.* **QE-17**(6), 965–969 (1981).
23. J. Koyama, H. Nishihara, M. Haruna, and T. Suhara, "Optical guide switches and their applications," in *Optical Guided-Wave Electronics*, by Editorial Committee of the Special Project Research on Optical Guided-Wave Electronics of Japan, Tokyo, 1981, pp. 419–431.